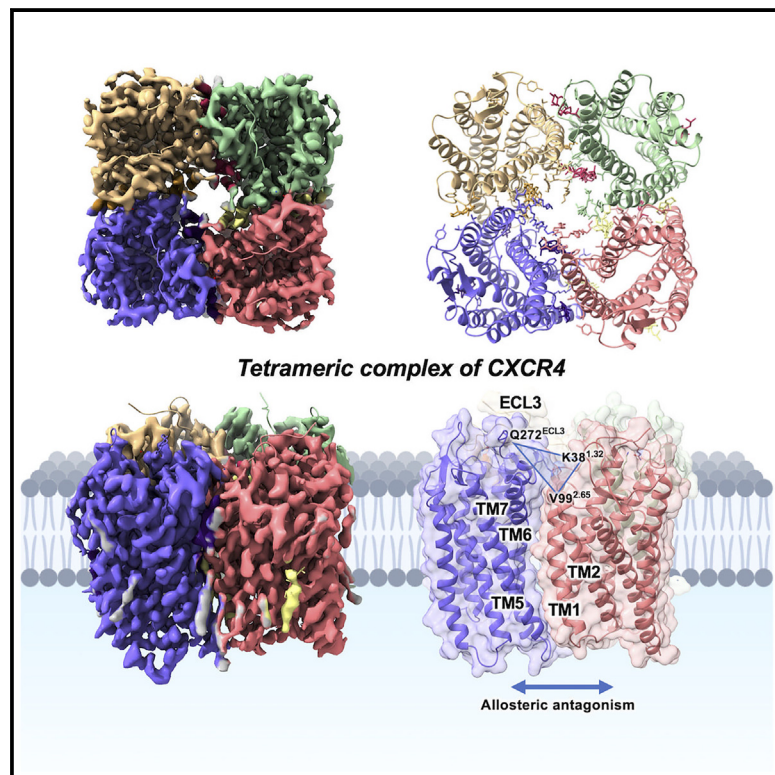


Structural basis of CXCR4 assembly and regulation

Graphical abstract



Authors

Aijun Liu, Yezhou Liu, Richard D. Ye

Correspondence

liuajun@cuhk.edu.cn (A.L.),
richardye@cuhk.edu.cn (R.D.Y.)

In brief

Liu et al. report a cryo-EM structure of the CXCR4 tetramer, with each protomer assembled into a rotationally symmetric arrangement. Structural and functional analyses demonstrate molecular interactions that stabilize the tetrameric architecture of CXCR4 via TM1/2 and TM5/6/7. These results suggest allosteric antagonism of CXCR4 through tetramerization.

Highlights

- Cryo-EM structure of a CXCR4 homo-tetramer with a unique rotationally symmetric arrangement
- Protomer interface consists of transmembrane helices TM1/2 and TM5/6/7
- Hydrogen bond triad of K38, V99, and Q272 stabilizes the tetrameric conformation
- An allosteric antagonism of GPCR demonstrated by CXCR4 homo-tetramer



Article

Structural basis of CXCR4 assembly and regulation

Aijun Liu,^{1,2,4,*} Yezhou Liu,^{1,2,4} and Richard D. Ye^{1,2,3,5,*}

¹Dongguan Songshan Lake Central Hospital, Dongguan Third People's Hospital, The Affiliated Dongguan Songshan Lake Central Hospital, Guangdong Medical University, Dongguan, Guangdong 523326, China

²Kobilka Institute of Innovative Drug Discovery, School of Medicine, The Chinese University of Hong Kong, Shenzhen, Guangdong 518172, China

³The Chinese University of Hong Kong, Shenzhen Futian Biomedical Innovation R&D Center, Shenzhen, Guangdong 518000, China

⁴These authors contributed equally

⁵Lead contact

*Correspondence: liuajun@cuhk.edu.cn (A.L.), richardye@cuhk.edu.cn (R.D.Y.)

<https://doi.org/10.1016/j.celrep.2025.115255>

SUMMARY

CXC chemokine receptor 4 (CXCR4) is a well-established drug target and a key representative of the chemokine receptor family. Chemokine receptors tend to assemble, and this assembly plays a critical role in regulating their functions. However, structural information regarding the organization of these receptors remains limited. Here, we present the cryoelectron microscopy (cryo-EM) structure of a CXCR4 homo-tetramer. In this tetramer, each protomer interfaces with adjacent protomers via TM1/2 and TM5/6/7, aligning at a 90° angle to assemble into a C4 rotationally symmetric arrangement. Each protomer allosterically regulates the others, with Q272 in the ECL3 loop interacting with K38 (TM1) and V99 (TM2) of the adjacent protomer, resulting in a mutually inhibitory configuration. These findings reveal an allosteric and antagonistic mechanism that prevents excessive activation, providing a structural framework for understanding the molecular mechanisms driving CXCR4 self-assembly and offering insights that could inspire further therapeutic strategies.

INTRODUCTION

CXC chemokine receptor 4 (CXCR4) is one of the earliest chemokine receptors identified and among the most extensively studied members of the chemokine receptor family. As a class A G protein-coupled receptor (GPCR), CXCR4 is essential for regulating diverse cellular processes, including lymphocyte trafficking,¹ hematopoiesis,² embryonic development, angiogenesis, and inflammation.^{3–5} Consequently, CXCR4 has emerged as an attractive therapeutic target, particularly in conditions such as epilepsy⁶, warts, hypo-gammaglobulinemia, infections, and myelokathexis syndrome^{6,7}; cancer metastasis⁸; and HIV infection.⁹

The structures of CXCR4 bound to antagonists have been resolved previously by crystallography, demonstrating homo- or hetero-dimeric forms.^{10,11} More recently, various class A GPCRs, including CXCR4, have been structurally characterized using cryoelectron microscopy (cryo-EM).^{12–18} These studies show the monomeric receptors coupled to G proteins in active conformation. Additionally, AI-based tools such as AlphaFold-Multimer have achieved precise predictions of the apo- and G protein-coupled structures of GPCRs, including chemokine receptors¹⁹ (Figure S1). However, these tools are ineffective at predicting chemokine receptor assembly into higher-order structures, such as the CXCR4 tetramer²⁰ (Figure S1). Thus, structural information on these assembled architectures remains largely unexplored. Notably, growing evidence indicates the presence of quaternary organization of chemokine receptors

on the plasma membrane in both homo- and hetero-oligomeric forms.^{21–30} Single-molecule fluorescence experiments have identified a dynamic equilibrium between monomeric, dimeric, and higher-order assemblies, which are critical for the regulation of receptor functions.^{31,32}

Both orthosteric and allosteric sites are critical for chemokine receptor functions. All endogenous ligands identified for chemokine receptors, such as CXCL12 for CXCR4, exclusively interact with the orthosteric site. In contrast, synthetic ligands have been discovered to bind to allosteric sites for modulation of the activities of chemokine receptors. Examples of CXCR4 include AMD11070³³ and AGR1.137.³⁴ In addition to ligands, the GPCR or part of it may serve as an allosteric modulator, as shown with pepducins, which are synthetic short peptides derived from the intracellular loop regions that have been found to effectively regulate CXCR4 activity through an allosteric mechanism.³⁵ Oligomerization of GPCRs makes it possible for the receptors to serve as natural allosteric modulators of their own function through formation of complex assemblies.^{21,29,30}

In this study, we present the high-resolution cryo-EM structure of a CXCR4 homo-tetramer, stabilized by both polar and nonpolar interactions between protomers, in the absence of a bound ligand or transducer proteins. The structure reveals an allosteric and mutual regulatory mechanism that prevents transducer protein coupling and maintains the receptor in an inactive state. This distinct arrangement allows each protomer to function as an allosteric “antagonist” for its neighboring protomers, representing a mutually inhibitory form of CXCR4. Through



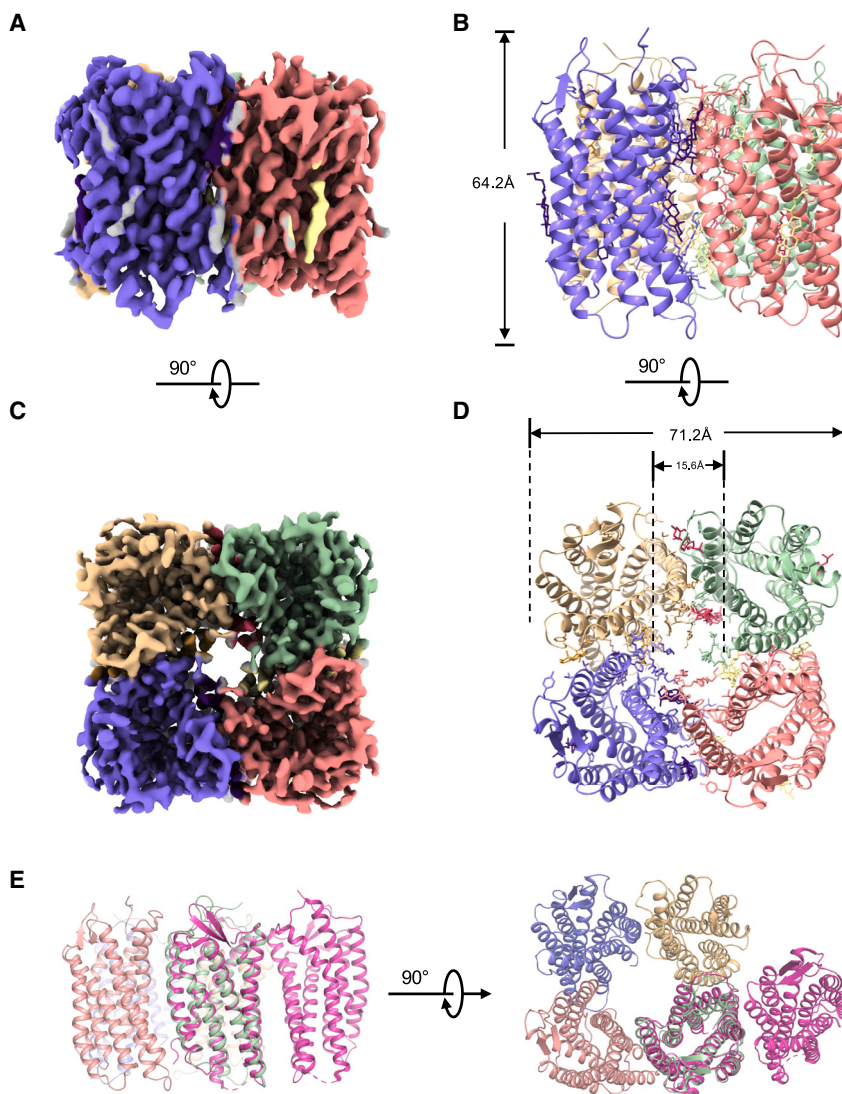


Figure 1. Overall structure of the CXCR4 tetramer

(A) Side view of the cryo-EM density map of the CXCR4 tetramer.
 (B) Side view of the coordinates of the CXCR4 tetramer.
 (C) Extracellular view of the cryo-EM density map of the CXCR4 tetramer.
 (D) Extracellular view of the coordinates of the CXCR4 tetramer.
 (E) Structural comparison of CXCR4 tetramer with the CXCR4 dimer in the inactive state (magenta; PDB: 3ODU).
 Lipids in (A)–(D) are shown as color sticks, detailed in the legend for Figure 3. See also Figures S1 and S2.

structural analysis and functional assays, we propose a stepwise mechanism for the assembly of CXCR4 tetramers and then conversion of the inactive oligomers to the functional monomers. Our findings provide a foundational framework for understanding the molecular mechanisms that drive the self-assembly of CXCR4 and possibly other chemokine receptors. Given the critical roles CXCR4 plays in health and disease, these insights could facilitate the development of regulatory agents targeting CXCR4.

RESULTS

Structural determination of the CXCR4 tetramer

The wild-type CXCR4 was cloned and recombinantly expressed using the baculovirus expression system together with other components, as detailed in **STAR Methods**. The CXCR4 complex from the primary peak of size-exclusion chromatography was purified and subjected to cryo-EM analysis (Figure S2A).

Cryo-EM micrographs revealed homogeneously distributed particles of the CXCR4 complex (Figure S2B), resulting in a high-resolution density map of 3.01 Å (Figures 1 and S3). The map displayed a homomeric tetramer architecture in which each protomer was arranged in parallel around a central axis to form a tightly packed C4 symmetry (Figures 1A and 1C). Notably, no apparent 2D average of other assemblies was observed in the 2D classification (Figure S2C), indicating a homogeneous tetramer composition of the purified CXCR4. Most residues could be unambiguously assigned based on the density map, with well-defined side chains in the 7 transmembrane (TM) helices as well as in the 3 intracellular loops and 3 extracellular loops (ECLs) (Figure S3). As with most reported GPCR structures, the flexible N termini and C termini were not clearly visible. Numerous lipid densities were identified at the central axis of the tetramer and at the interfaces of the protomers (Figures 1A–1D), presumably stabilizing the tetrameric complex structure.

The assembly of CXCR4 into a mutually locking inhibitory tetramer

The CXCR4 tetramer assembles as a stable disk with a thickness of about 65 Å and a diameter of approximately 70 Å (Figures 1B and 1D), forming a central pore with a diameter of around 15 Å (Figure 1D). Interestingly, the central channel appears to be filled with lipids based on the EM map (Figures 1A–1D), although the densities in the central cavity are not well assigned due to intrinsic flexibility of the lipids (Figures 1A, 1B, and S3C). The lipids surrounding the CXCR4 tetramer are clearly defined, showing appropriate interactions that may help to stabilize the tetramer conformation.

The assembly of a tetramer differs from that of a dimer for CXCR4. In the CXCR4 tetramer, each protomer forms two

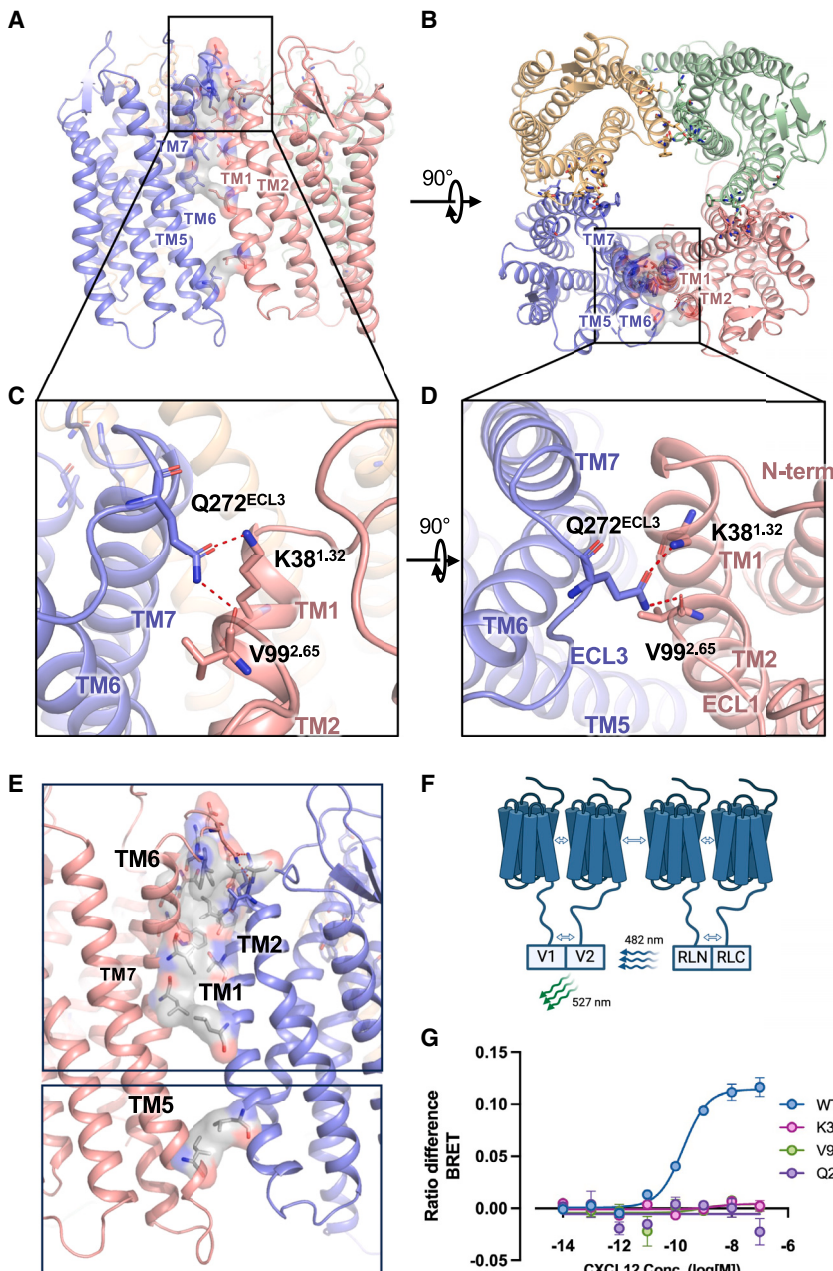


Figure 2. The assembly and interface interactions of the CXCR4 tetramer

(A and C) Side views of the polar interactions between the protomers in the CXCR4 tetramer.

(B and D) Extracellular views of the polar interactions between the protomers in the CXCR4 tetramer.

(E) Polar (colored) and non-polar (gray) interactions at the CXCR4 tetramer interface.

(F) Schematic of the complementary BRET assay. V1 (1–210 of mVenus), V2 (211–238 of mVenus), RLN (1–228 of RLuc), and RLC (229–311 of RLuc) are fused to the C terminus of CXCR4. RLuc (RLN+RLC) is the BRET donor with emission wavelength (Em) of 482 nm, and mVenus (V1+V2) (Em. 527 nm) is the BRET acceptor.

(G) The complementary BRET assay readouts for wild-type CXCR4 and mutants. The BRET ratio is calculated as Em_{527}/Em_{460} , and the BRET difference is calculated as $\Delta BRET = (\text{average } BRET_{\text{after stimulation}}) - (\text{average } BRET_{\text{before stimulation}})$. Shown are means \pm SEM from 3 independent experiments, each with duplicate measurements. See also Figure S4.

a drug candidate in clinical trials, cannot be overcome by the native ligand CXCL12,³³ suggesting a distinct structural mechanism underlying allosteric regulation in contrast to orthosteric regulation.

The interface of the CXCR4 tetramer

The packing of the CXCR4 tetramer mainly involves TM1 and TM2 of one protomer and TM5, TM6, and TM7 of the other protomer (Figures 2A and 2B). Notably, these key TM helices, particularly TM6 and TM7, are widely recognized as crucial regions for class A GPCR activation and serve as key sites for allosteric modulation.^{36–38} The outward movement of TM6, which is the conserved and indispensable conformational change leading to activation, allows for G protein or β -arrestin coupling and subsequent signal

distinct interfaces with the adjacent protomers, which align at a 90° angle and create a C4 rotationally symmetric structure. The interfaces in the tetramer differ markedly from those observed in the CXCR4 dimers in a previous crystallization study.¹⁰ No overlap between the interfaces was observed when these structures were aligned (Figure 1E). Notably, the CXCR4 dimer was formed by binding to an orthosteric antagonist, which blocks native chemokine binding by occupying the binding sites. However, structural data for CXCR4 bound to allosteric antagonists such as AMD11070³³ and AGR1.137³⁴ or to allosteric modulators such as pepducins remain unavailable. Unlike orthosteric antagonists, the potent allosteric inhibitory effect of AMD11070,

transduction. These TM helices are also the primary targets of existing drug candidates for CXCR4. The binding of allosteric ligands to these regions may affect the assembly of CXCR4, thereby modulating receptor functions.

Hydrophobic effects predominantly contribute to the stabilization of the tetrameric conformation at the protomer interface (Figures 2A and 2B). Extensive nonpolar interactions are observed between TM1/2 of one protomer and TM5/6/7 of the other (Figure 2E). Polar interactions further enhance the interaction by forming hydrogen bonds between Q272^{ECL3} of one protomer and K38^{1,32} and V99^{2,65} of the other (Figures 2C and 2D). The hydrogen bond triad tightly holds the ECL3 of one

protomer with TM1 and TM2 of the adjacent protomer, thereby stabilizing the tetrameric architecture.

To verify these interactions at the interface, we introduced a complementary bioluminescence resonance energy transfer (BRET) assay. *Renilla* luciferase (RLuc) as the BRET donor is separated into an N-terminal fragment (RLN; 1–228 of RLuc) and a C-terminal fragment (RLC; 229–311 of RLuc)^{39,40} and then linked to the C terminus of the receptor. mVenus as the BRET acceptor was separated into V1 (1–210 of mVenus) and V2 (211–238 of mVenus) fragments^{39,40} and connected to the C termini of the receptors. When these receptor monomers approached each other, complementation of RLuc and mVenus occurs simultaneously, producing functional proteins for BRET, as illustrated in Figure 2F. Upon CXCL12 ligand stimulation, the BRET ratio of the complementary system increased, reflecting formation of the CXCR4 tetramer (Figure 2G). When alanine substitution was introduced at K38^{1,32}, V99^{2,65}, and Q272^{ECL3}, the CXCL12-induced increase in BRET ratio was abrogated (Figure 2G). The cell-surface expression levels of the mutants were comparable to that of wild-type CXCR4 (Figure S4). Furthermore, these mutants could still mediate cyclic AMP inhibition response with an amplitude comparable to that of the wild-type CXCR4 (Figure S4). Taken together, these experimental results indicate that the alanine substitutions abrogated formation of the CXCR4 tetramer but did not affect the ability of the resulting CXCR4 to transduce signals through Gi coupling. This result supports involvement of K38^{1,32}, V99^{2,65}, and Q272^{ECL3}, critical for the hydrogen bond triad, in the formation of CXCR4 tetramers.

Cholesterols and native lipids stabilize the CXCR4 tetramer

Lipid densities were found in the central hole and around the protomer interface, possibly acting as the molecular glue to form hydrophobic networks that stabilize the CXCR4 tetramer. There are 5 cholesterol molecules (CLR 1–5) and 2 other membrane lipid molecules (PGT1 and PGT2) clearly identified at the interface of each protomer, constituting, in total, 20 cholesterol molecules and 8 other membrane lipid molecules in the tetramer structure (Figure 3).

For cholesterol molecules, CLR1, CLR3, and CLR4 are accommodated in the interface between protomers. CLR2 lies between TM6 and TM7, and CLR5 is situated in a cavity formed by TM2 and TM4 (Figures 3A–3J). CLR1 is positioned near the extracellular region and forms hydrophobic interactions with F36^{1,30}, F40^{1,34}, and F293^{7,44} of one protomer (colored salmon) and K282^{7,33}, W283^{7,34}, and I286^{7,37} of the other (colored slate blue) (Figures 3A and 3B). CLR2 has hydrophobic effects with A250^{6,46}, C251^{6,47}, L290^{7,41}, and L297^{7,48} (Figures 3C and 3D). CLR3 is also close to the extracellular region, holding together residues S46^{1,40}, V96^{2,62}, and V99^{2,65} of one receptor monomer and L208^{5,47}, I257^{6,53}, I261^{6,57}, F264^{6,60}, I269^{ECL3}, and I270^{ECL3} of the other through nonpolar interactions (Figures 3E and 3F). CLR4 resides near the intracellular region of the receptor, forming nonpolar interactions with T51^{1,45}, G55^{1,49}, L58^{1,52}, V59^{1,53}, V62^{1,56}, P299^{7,50}, Y302^{7,53}, and A303^{7,54} in the receptor protomer but no interaction with the other receptor protomer (Figures 3G and 3H). CLR5 has hydrophobic interactions with

V82^{2,48}, L86^{2,52}, W161^{4,50}, and L165^{4,54} (Figures 3I and 3J). Since cholesterol is a key component of lipid rafts on the cell membrane and modulates organization of membrane proteins, these nonpolar interactions between cholesterol and receptor protomers are expected to stabilize the tetramer architecture of CXCR4. The density of cholesterol molecules also regulates membrane fluidity, possibly favoring the formation of the CXCR4 tetramer.

For the membrane lipid molecules, PGT1 and PGT2 are located in the interface of adjacent CXCR4 protomers (Figures 3K and 3N). PGT1 forms a hydrogen bond with N35^{1,29} and hydrophobic interactions with F36^{1,30} (Figures 3K and 3L). PGT2 forms extensive nonpolar interactions with G212^{5,51}, I215^{5,54}, Y219^{5,58}, K239^{6,35}, V242^{6,38}, and L246^{6,42} of one protomer and I223^{5,62}, I300^{7,51}, and F304^{7,55} of the other (Figures 3M and 3N). These lipid molecules together act as a molecular glue to hold receptor protomers together in the CXCR4 tetramer. Further studies featuring the detailed role of lipids in the regulation of CXCR4 tetramerization would be of great interest.

Allosteric regulation of the CXCR4 tetramer

The structure of protomers in the CXCR4 tetramer was compared with the reported CXCR4 structures in the active state (PDB: 8K3Z)¹² and inactive state (PDB: 3ODU).¹⁰ The protomer in the CXCR4 tetramer shows a significant difference from the CXCR4 monomer in the active state (Figures 4A, 4B, and S5). In the CXCR4 tetramer, TM6 of the protomer bends inwards and its TM5 moves outward, and TM7 shows an outward displacement when compared with monomeric CXCR4 in the active state (Figure 4A). The extracellular top of TM1 in the CXCR4 tetramer shows an outward movement, and ECL2 of the protomer in the CXCR4 tetrameric structure moves inward (Figures 4B; S5). These conformational characteristics demonstrate a stable inhibitory state of the CXCR4 tetramer.

The CXCR4 protomer in the tetramer was further compared with the reported structure in the inactive state (Figure 4C). The extracellular end of TM1 exhibited an outward movement (Figure 4C). Moreover, ECL2 moved inwards, and the extracellular proximities of TM6 and TM7 showed an inward rotation (Figure 4C). Additionally, the intracellular end of TM6 bent slightly inward (Figure 4C). These comparisons highlight the conformational differences of the protomer involved in maintaining the inactive state through allosteric rather than orthosteric induction.

Looking into the key motifs for GPCR activation, including the Asp-Arg-Tyr (DRY) ionic lock, NPxxY motif, CWxP motif, and P-I-F motif, we found that the side-chain conformations of these motifs in CXCR4 tetramers demonstrate an inactive state (Figures 4D–4G). For the DRY motif, which functions as an ionic lock for Gαi binding to the receptor, the side chain of R^{3,50} was pointing downwards and blocking the intracellular G protein binding pocket of the receptor (Figure 4D). For the CWxP motif, which serves as an essential trigger for orthostERICALLY induced conformational changes and signal transduction, the side-chain conformations remained largely similar despite an inward bend of TM6 (Figure 4E). The P-I-F motif is replaced by P-V-F in CXCR4, with consistent side-chain orientations between the tetramer protomer and the inactive state structure (Figure 4F).

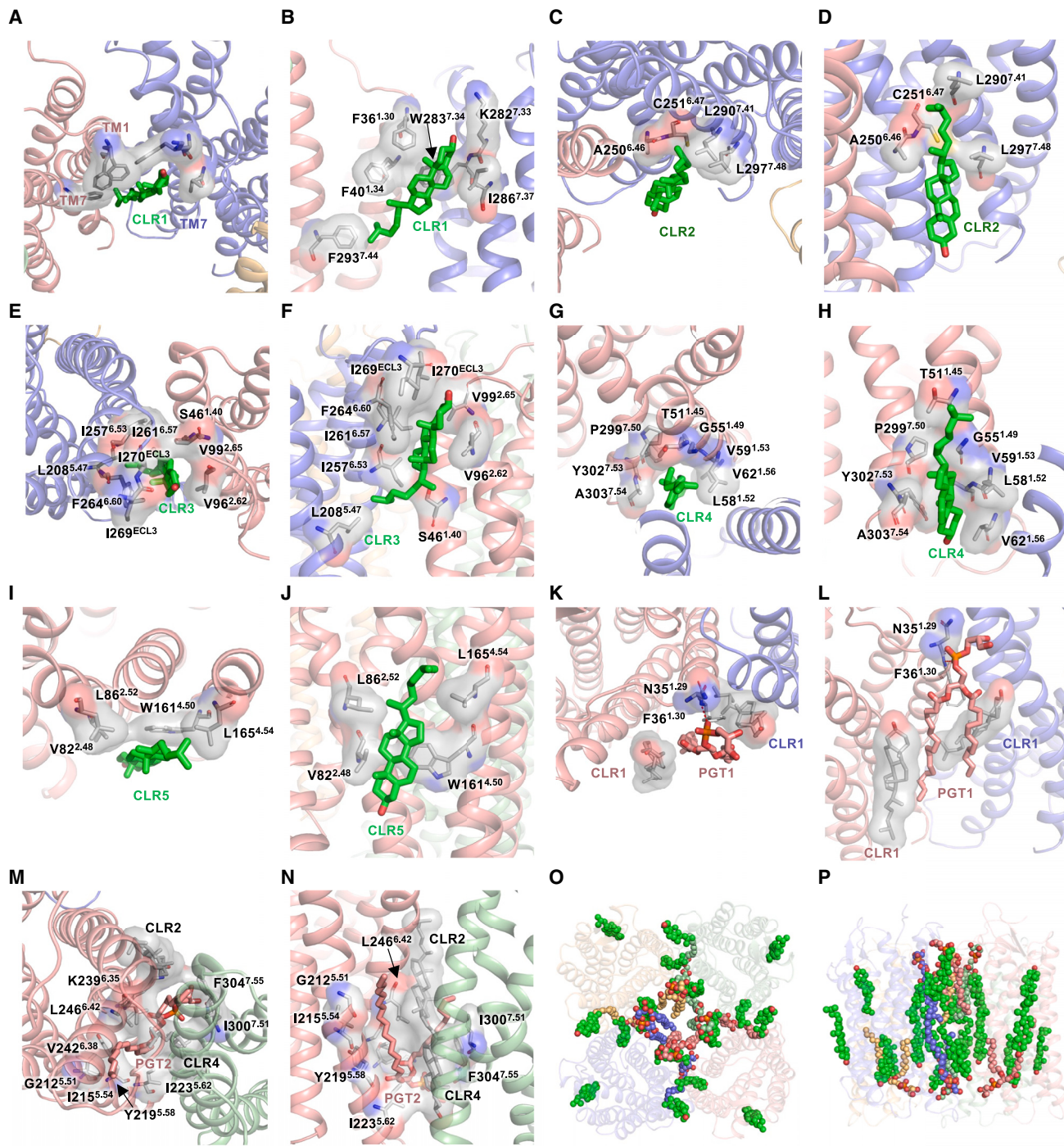


Figure 3. Lipids in the CXCR4 tetramer

(A–J) CXCR4 interaction with cholesterol (CLR; green and grouped in numbers), viewed from the top (A, C, E, G, and I) and from the side (B, D, F, H, and J). (K–L) CXCR4 interaction with other membrane lipids (PGT, salmon and grouped in numbers), viewed from the top (K and M) and from the side (L and N). (O and P) Overview of lipids in the CXCR4 tetramer, viewed from the top (O) and from the side (P).

The NPxxY motif exhibited differences in side-chain conformation between the protomer and inactive structure, presumably due to TM7 displacement to accommodate adjacent protomers (Figure 4E). Altogether, these comparisons demonstrate that the

tetrameric architecture of CXCR4 represents an inactive state of the receptor or, more precisely, a self-inhibitory state.

The CXCR4 tetramer reveals an allosteric inhibitory state through homomeric assembly and regulation. The interfaces of

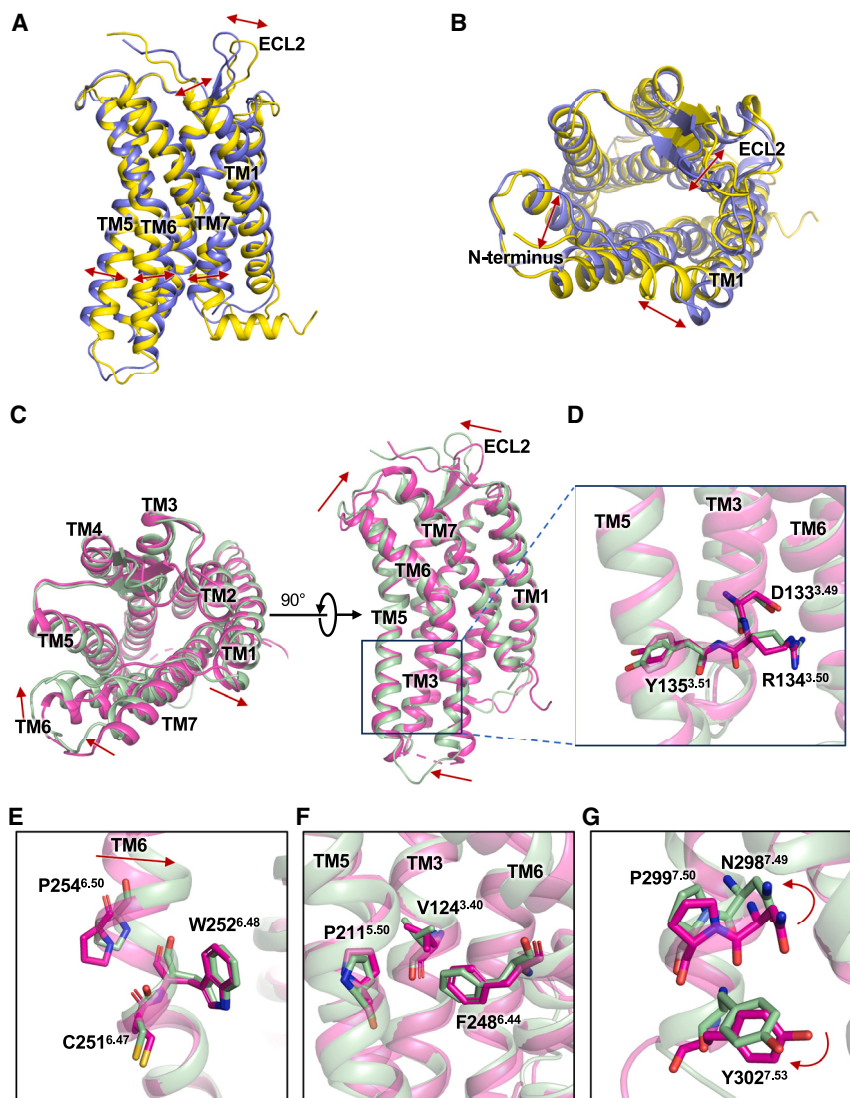


Figure 4. Comparisons of conformations between the CXCR4 tetramer and CXCR4 dimer in the inactive state

(A and B) Structural comparison between the protomer in the CXCR4 tetramer (slate blue) and the active-state CXCR4 (yellow; PDB: 8K3Z).

(C) Superimposed structure of the CXCR4 tetramer (pale green) and the CXCR4 dimer in the inactive state (magenta; PDB: 3ODU).

(D) Comparison of the DRY motif conformations of the CXCR4 tetramer and dimer.

(E–G) Comparison of the CWxF motif (E), P-V-F motif (F), and NPxxY motif (G). The red arrow in (E) illustrates an inward shift of TM6 in the tetramer CXCR4. The red arrows in (G) indicate rotamer conformation changes at N^{7.49} and Y^{7.53}.

See also Figure S5.

one receptor can further stabilize the allosteric pocket formed by TM1 and TM2 of its adjacent receptor (Figures 5B and 5E). This triangular allosteric site network in the CXCR4 tetrameric architecture provides a solid foundation for allosteric antagonism mediated by the protomers.

DISCUSSION

Chemokine receptors form quaternary structures to regulate a wide range of physiological functions.^{32,42–44} The quaternary architecture of protomers is affected by interactions between chemokines and chemokine receptors, which influence various spatiotemporal aspects of chemotactic responses.^{22,31,45,46} The constitutive activation of chemokine receptors leads to increased basal activity that correlates with their expression levels. In this study, we report the forma-

the tetrameric form of CXCR4 is rather different from that of dimeric CXCR4, which is preferentially induced by orthosteric antagonists (Figure 5A).^{10,41} Moreover, compared with our recently resolved CXCL12-CXCR4-Gi protein complex structure,¹² the tetrameric CXCR4 cannot accommodate G protein binding to the cytoplasmic pocket (Figures 5C and 5D). The mutually locking inhibitory architecture represents allosteric antagonism to prevent excessive activation, as no endogenous antagonist was found for CXCR4 to offset increased receptor signaling resulting from its increasing expression levels (Figure 5B). The protomers are held together through hydrogen bonds between Q272^{ECL3} in one protomer and K38^{1,32} and V99^{2,65} in the adjacent protomer. In this manner, ECL3 and TM5–TM7 of one protomer are securely linked to TM1 and TM2 of the next protomer, facilitating stabilization of the tetrameric architecture in its inactive conformation. TM1 and TM2 of one protomer also allosterically modulate the adjacent protomer by restricting the movement of TM5–TM7, thereby inhibiting receptor activation. TM5–TM7 of

formation of CXCR4 homomeric tetramers in a parallel and symmetric form, unveiling a self-inhibitory mechanism by which the specific assembly helps to maintain the receptor in an inactive state, thereby preventing excessive activation. This distinct arrangement allows each protomer to occupy the allosteric site of the adjacent receptor, acting as a non-classical “allosteric antagonist.”

The monomeric form of chemokine GPCRs, including CXCR4, is coupled to the Gi proteins for TM signaling.¹² In comparison, the oligomeric assembly of GPCRs, as shown in the CXCR4 tetramer, serves to regulate the availability of functional receptor monomers.^{21,26,31,47} It has been shown that the regulation of CXCR4 requires dynamic formation of higher-order oligomers^{21,26,31,41,47} and a dynamic assembly cycle involving conformational changes in different CXCR4 oligomerization states (Figure S6). Early studies demonstrated that CXCR4 exists as a constitutive oligomer on the cell surface.^{44,48} For receptor activation, the chemokine ligand CXCL12 binds to CXCR4 and

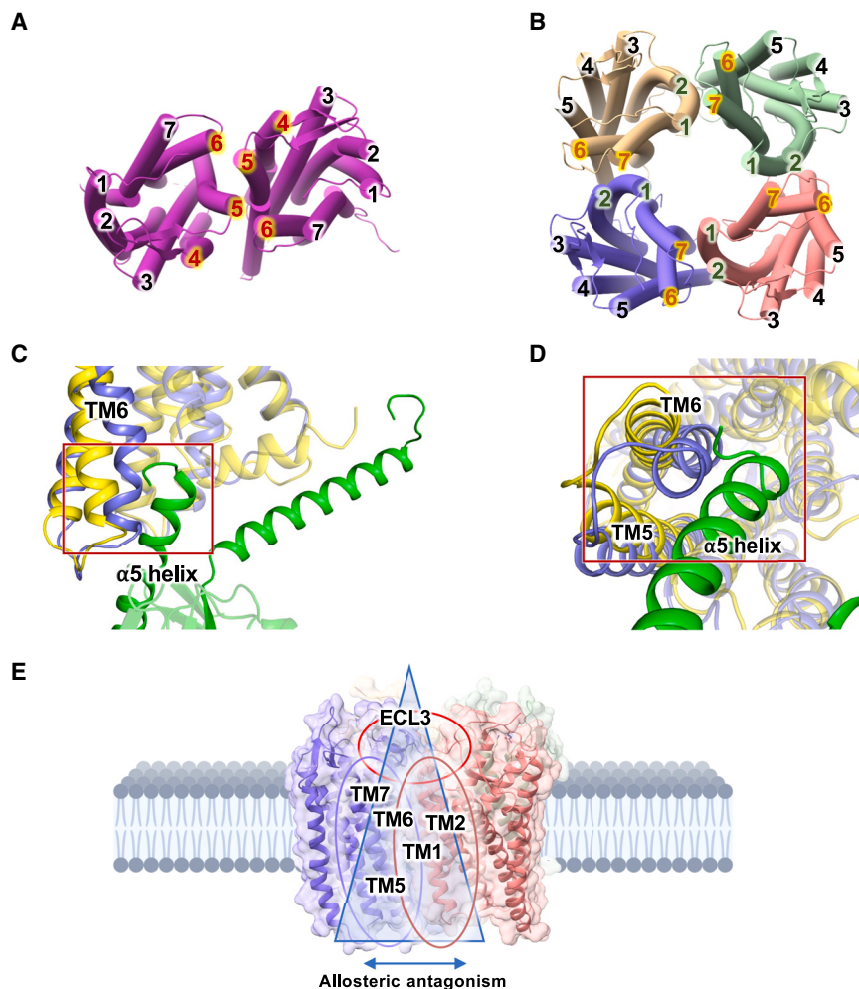


Figure 5. Mechanism of CXCR4 tetramer assembly

(A) Extracellular view of the CXCR4 dimer structure (PDB: 3ODU). The interacting TM helices are highlighted and numbered.

(B) Extracellular view of the CXCR4 tetramer structure. The interacting TM helices are highlighted with numbers.

(C and D) Comparison of the Gi interface conformations between the protomer in the CXCR4 tetramer (blue) and the active-state CXCR4 (yellow). Gi α is shown in green.

(E) Illustration of allosteric antagonism mediated between protomers within the tetrameric CXCR4. The red circle highlights the polar interaction triad between ECL3 of one protomer and TM1 and TM2 of the adjacent protomer. The purple circle represents the TM5-TM7 allosteric site, and the dark pink circle represents the TM1 and TM2 allosteric sites. The blue triangle indicates the network of allosteric sites between receptor protomers. See also Figures S6 and S7.

forms a monomeric G protein-coupled signaling complex. After receptor activation and G protein signaling, β -arrestin binds to CXCR4, desensitizes the receptor, and induces receptor internalization and membrane recycling.⁴⁹ A more recent study suggests that CXCR4 oligomers tend to internalize more easily than monomers.⁴⁵ Therefore, the tetrameric state of CXCR4 may represent the assembly of inactive-state CXCR4 prior to the ligand-induced receptor activation and G protein signaling as well as during receptor internalization and intracellular membrane trafficking and recycling. The tetrameric architecture of CXCR4 represents an important mechanism for allosteric regulation through mutual locking inhibition of the receptor. This form of allosteric antagonism regulates the availability of functional CXCR4 monomers, thus affecting the functions of CXCR4 and its associated cellular activities.^{28,31,32}

Receptor oligomerization is a common feature among chemokine receptors. Homo- and hetero-oligomeric assemblies of chemokine receptors are regulated by cell-surface expression levels as well as the level of their corresponding ligands.⁵⁰ With the key sites for tetramerization found in this study, we further questioned whether these interacting residues between protomers are conserved among chemokine receptors. Interestingly,

K38^{1,32} is conserved in ACKR2, ACKR4, CCR8, CXCR1, CXCR2, CXCR4, and CXCR6. V99^{2,65} is found in ACKR4, CXCR1, CXCR2, and CXCR4. Q272^{ECL3}, however, is unique for CXCR4 (Figure S7). Therefore, the key sites for CXCR4 tetramerization are partially conserved among chemokine receptors, suggesting that different forms of higher-order oligomeric assembly may exist for different chemokine receptors. Indeed, a recent report on the structure of a homotrimeric complex of UL78, a virally encoded chemokine receptor, adds insights into different

forms of receptor oligomeric states among the chemokine receptors.⁵¹ The homotrimeric UL78 shows a triangular architecture, making the complex compact with no extra space in the centroid. TM3-TM6 are primarily responsible for molecular interactions between protomers. This compact arrangement of the UL78 homotrimer, distinct from our tetrameric CXCR4 complex with a hole-like centroid, may support its unique conformation, which is different from both the active and inactive state of GPCRs.

In summary, the present study provides a structural perspective of CXCR4 allosteric regulation through tetramer formation and identifies key sites involved. These findings could inspire additional therapeutic strategies targeting CXCR4. For example, ligands that effectively bind to the interaction sites at CXCR4 tetramer assembly interfaces could serve as potent regulators of CXCR4 activity, similar to many successful allosteric modulatory drugs that have been developed.

Limitations of the study

The high-resolution tetrameric structure of CXCR4 provides previously unavailable insights into the higher-order oligomeric assembly of a GPCR, but the mechanisms regarding the

membrane dynamics for the assembly and dissociation of CXCR4 tetramer remain largely unknown. Further studies will be necessary to characterize the dynamic feature of the CXCR4 oligomeric state and its physiological relevance *in vitro* and *in vivo*.

RESOURCE AVAILABILITY

Lead contact

Requests for further information, resources, and reagents should be directed to and will be fulfilled by the lead contact, Richard D. Ye (richardye@cuhk.edu.cn).

Materials availability

All stable reagents generated in this study are available from the [lead contact](#) without restriction. All plasmids and cell lines generated in this study are available from the [lead contact](#) with a completed materials transfer agreement.

Data and code availability

- The cryo-EM density map of the CXCR4 tetrameric complex resolved in this study and the associated atomic coordinates have been deposited in the Electron Microscopy Data Bank (EMDB: EMD-39573) and in the Protein Data Bank (PDB: 8YU7), respectively. They are publicly available as of the date of publication. Accession numbers are listed in the [key resources table](#).
- This paper does not report original code.
- Any additional information required to reanalyze the data reported in this work paper is available from the [lead contact](#) upon request.

ACKNOWLEDGMENTS

This work was supported by National Natural Science Foundation of China 82402140 (to A.L.) and 32070950 (to R.D.Y.), Special Project for Clinical and Basic Sci & Tech Innovation of Guangdong Medical University GDMULCJC2024121 and GDMULCJC2024156 (to A.L.), Science, Technology and Innovation Commission of Shenzhen Municipality grant GXWD20201231105722002-20200831175432002 (to R.D.Y.), and Shenzhen Science and Technology Program grant RCBS20221008093330067 (to A.L.). This work was also supported by National Key R&D Program of China grant 2019YFA0906003 (to R.D.Y.); Yunnan Key Research and Development Program grant 202402AA310032 (to R.D.Y.); Shenzhen Medical Research Fund SMRF-D2403009 (to R.D.Y.); the Kobilka Institute of Innovative Drug Discovery at The Chinese University of Hong Kong, Shenzhen (to R.D.Y.); the Ganghong Young Scholar Development Fund (to R.D.Y.); China Postdoctoral Science Foundation 2022M713049 (to A.L.); start-up funds from Dongguan Songshan Lake Central Hospital (to A.L.); and Shenzhen-Hong Kong Cooperation Zone for Technology and Innovation grant HZQB-KCZYB-2020056 (to R.D.Y.).

AUTHOR CONTRIBUTIONS

A.L. and R.D.Y. conceived, initiated, and designed the project. A.L. and Y.L. performed the experiments, analyzed the data, and prepared the figures. A.L. and R.D.Y. supervised the research and wrote the manuscript with input from Y.L.

DECLARATION OF INTERESTS

The authors declare no competing interests.

STAR★METHODS

Detailed methods are provided in the online version of this paper and include the following:

- KEY RESOURCES TABLE
- EXPERIMENTAL MODEL AND STUDY PARTICIPANT DETAILS

● METHOD DETAILS

- Constructs
- Protein expression
- Complex purification
- Cryo-EM grid preparation
- Cryo-EM data collection
- Cryo-EM image processing and 3D reconstruction
- Model building and refinement
- Complementary BRET assay
- Surface expression analysis
- cAMP inhibition assay

● QUANTIFICATION AND STATISTICAL ANALYSIS

SUPPLEMENTAL INFORMATION

Supplemental information can be found online at <https://doi.org/10.1016/j.celrep.2025.115255>.

Received: September 27, 2024

Revised: December 17, 2024

Accepted: January 10, 2025

Published: January 31, 2025

REFERENCES

1. De Filippo, K., and Rankin, S.M. (2018). CXCR4, the master regulator of neutrophil trafficking in homeostasis and disease. *Eur. J. Clin. Invest.* 48 Suppl 2, e12949. <https://doi.org/10.1111/eci.12949>.
2. Sugiyama, T., Kohara, H., Noda, M., and Nagasawa, T. (2006). Maintenance of the hematopoietic stem cell pool by CXCL12-CXCR4 chemokine signaling in bone marrow stromal cell niches. *Immunity* 25, 977–988. <https://doi.org/10.1016/j.immuni.2006.10.016>.
3. Doranz, B.J., Orsini, M.J., Turner, J.D., Hoffman, T.L., Berson, J.F., Hoxie, J.A., Peiper, S.C., Brass, L.F., and Doms, R.W. (1999). Identification of CXCR4 domains that support coreceptor and chemokine receptor functions. *J. Virol.* 73, 2752–2761. <https://doi.org/10.1128/JVI.73.4.2752-2761.1999>.
4. Feng, Y., Broder, C.C., Kennedy, P.E., and Berger, E.A. (1996). HIV-1 entry cofactor: functional cDNA cloning of a seven-transmembrane, G protein-coupled receptor. *Science* 272, 872–877. <https://doi.org/10.1126/science.272.5263.872>.
5. Salvatore, P., Pagliarulo, C., Colicchio, R., and Napoli, C. (2010). CXCR4-CXCL12-Dependent Inflammatory Network and Endothelial Progenitors. *Curr. Med. Chem.* 17, 3019–3029.
6. Balabanian, K., Levoye, A., Klemm, L., Lagane, B., Hermine, O., Harriague, J., Baleux, F., Arenzana-Seisdedos, F., and Bachelerie, F. (2008). Leukocyte analysis from WHIM syndrome patients reveals a pivotal role for GRK3 in CXCR4 signaling. *J. Clin. Invest.* 118, 1074–1084. <https://doi.org/10.1172/JCI33187>.
7. Heusinkveld, L.E., Majumdar, S., Gao, J.L., McDermott, D.H., and Murphy, P.M. (2019). WHIM Syndrome: from Pathogenesis Towards Personalized Medicine and Cure. *J. Clin. Immunol.* 39, 532–556. <https://doi.org/10.1007/s10875-019-00665-w>.
8. Smit, M.J., Schlecht-Louf, G., Neves, M., van den Bor, J., Penela, P., Sidemius, M., Bachelerie, F., and Mayor, F., Jr. (2021). The CXCL12/CXCR4/ACKR3 Axis in the Tumor Microenvironment: Signaling, Crosstalk, and Therapeutic Targeting. *Annu. Rev. Pharmacol. Toxicol.* 61, 541–563. <https://doi.org/10.1146/annurev-pharmtox-010919-023340>.
9. Bleul, C.C., Farzan, M., Choe, H., Parolin, C., Clark-Lewis, I., Sodroski, J., and Springer, T.A. (1996). The lymphocyte chemoattractant SDF-1 is a ligand for LESTR/fusin and blocks HIV-1 entry. *Nature* 382, 829–833. <https://doi.org/10.1038/382829a0>.
10. Wu, B., Chien, E.Y.T., Mol, C.D., Fenalti, G., Liu, W., Katritch, V., Abagyan, R., Brooun, A., Wells, P., Bi, F.C., et al. (2010). Structures of the CXCR4

- chemokine GPCR with small-molecule and cyclic peptide antagonists. *Science* 330, 1066–1071. <https://doi.org/10.1126/science.1194396>.
11. Qin, L., Kufareva, I., Holden, L.G., Wang, C., Zheng, Y., Zhao, C., Fenalti, G., Wu, H., Han, G.W., Cherezov, V., et al. (2015). Crystal structure of the chemokine receptor CXCR4 in complex with a viral chemokine. *Science* 347, 1117–1122. <https://doi.org/10.1126/science.1261064>.
 12. Liu, Y., Liu, A., Li, X., Liao, Q., Zhang, W., Zhu, L., and Ye, R.D. (2024). Cryo-EM structure of monomeric CXCL12-bound CXCR4 in the active state. *Cell Rep.* 43, 114578. <https://doi.org/10.1016/j.celrep.2024.114578>.
 13. Ishimoto, N., Park, J.H., Kawakami, K., Tajiri, M., Mizutani, K., Akashi, S., Tame, J.R.H., Inoue, A., and Park, S.Y. (2023). Structural basis of CXC chemokine receptor 1 ligand binding and activation. *Nat. Commun.* 14, 4107. <https://doi.org/10.1038/s41467-023-39799-2>.
 14. Liu, K., Wu, L., Yuan, S., Wu, M., Xu, Y., Sun, Q., Li, S., Zhao, S., Hua, T., and Liu, Z.J. (2020). Structural basis of CXC chemokine receptor 2 activation and signalling. *Nature* 585, 135–140. <https://doi.org/10.1038/s41586-020-2492-5>.
 15. Jiao, H., Pang, B., Liu, A., Chen, Q., Pan, Q., Wang, X., Xu, Y., Chiang, Y.C., Ren, R., and Hu, H. (2024). Structural insights into the activation and inhibition of CXC chemokine receptor 3. *Nat. Struct. Mol. Biol.* 31, 610–620. <https://doi.org/10.1038/s41594-023-01175-5>.
 16. Yen, Y.C., Schafer, C.T., Gustavsson, M., Eberle, S.A., Dominik, P.K., Deneka, D., Zhang, P., Schall, T.J., Kossiakoff, A.A., Tesmer, J.J.G., and Handel, T.M. (2022). Structures of atypical chemokine receptor 3 reveal the basis for its promiscuity and signaling bias. *Sci. Adv.* 8, eabn8063. <https://doi.org/10.1126/sciadv.abn8063>.
 17. Zhang, H., Chen, K., Tan, Q., Shao, Q., Han, S., Zhang, C., Yi, C., Chu, X., Zhu, Y., Xu, Y., et al. (2021). Structural basis for chemokine recognition and receptor activation of chemokine receptor CCR5. *Nat. Commun.* 12, 4151. <https://doi.org/10.1038/s41467-021-24438-5>.
 18. Shao, Z., Tan, Y., Shen, Q., Hou, L., Yao, B., Qin, J., Xu, P., Mao, C., Chen, L.N., Zhang, H., et al. (2022). Molecular insights into ligand recognition and activation of chemokine receptors CCR2 and CCR3. *Cell Discov.* 8, 44. <https://doi.org/10.1038/s41421-022-00403-4>.
 19. Abramson, J., Adler, J., Dunger, J., Evans, R., Green, T., Pritzel, A., Ronneberger, O., Willmore, L., Ballard, A.J., Bambrick, J., et al. (2024). Accurate structure prediction of biomolecular interactions with AlphaFold 3. *Nature* 630, 493–500. <https://doi.org/10.1038/s41586-024-07487-w>.
 20. Di Marino, D., Conflitti, P., Motta, S., and Limongelli, V. (2023). Structural basis of dimerization of chemokine receptors CCR5 and CXCR4. *Nat. Commun.* 14, 6439. <https://doi.org/10.1038/s41467-023-42082-z>.
 21. Milligan, G., Ward, R.J., and Marsango, S. (2019). GPCR homo-oligomerization. *Curr. Opin. Cell Biol.* 57, 40–47. <https://doi.org/10.1016/j.ceb.2018.10.007>.
 22. Ward, R.J., Pediani, J.D., Marsango, S., Jolly, R., Stoneman, M.R., Biener, G., Handel, T.M., Raicu, V., and Milligan, G. (2021). Chemokine receptor CXCR4 oligomerization is disrupted selectively by the antagonist ligand IT1t. *J. Biol. Chem.* 296, 100139. <https://doi.org/10.1074/jbc.RA120.016612>.
 23. Munoz, L.M., Lucas, P., Holgado, B.L., Barroso, R., Vega, B., Rodriguez-Frade, J.M., and Mellado, M. (2011). Receptor oligomerization: a pivotal mechanism for regulating chemokine function. *Pharmacol. Ther.* 131, 351–358. <https://doi.org/10.1016/j.pharmthera.2011.05.002>.
 24. Sohy, D., Yano, H., de Nadai, P., Urizar, E., Guillabert, A., Javitch, J.A., Parmentier, M., and Springael, J.Y. (2009). Hetero-oligomerization of CCR2, CCR5, and CXCR4 and the protean effects of “selective” antagonists. *J. Biol. Chem.* 284, 31270–31279. <https://doi.org/10.1074/jbc.M109.054809>.
 25. Cordomi, A., Navarro, G., Aymerich, M.S., and Franco, R. (2015). Structures for G-Protein-Coupled Receptor Tetramers in Complex with G Proteins. *Trends Biochem. Sci.* 40, 548–551. <https://doi.org/10.1016/j.tibs.2015.07.007>.
 26. Martínez-Muñoz, L., Villares, R., Rodríguez-Fernández, J.L., Rodríguez-Frade, J.M., and Mellado, M. (2018). Remodeling our concept of chemokine receptor function: From monomers to oligomers. *J. Leukoc. Biol.* 104, 323–331. <https://doi.org/10.1002/jbl.2m1217-503>.
 27. Palczewski, K. (2010). Oligomeric forms of G protein-coupled receptors (GPCRs). *Trends Biochem. Sci.* 35, 595–600. <https://doi.org/10.1016/j.tibs.2010.05.002>.
 28. Paradis, J.S., Feng, X., Murat, B., Jefferson, R.E., Sokrat, B., Szpakowska, M., Hogue, M., Bergkamp, N.D., Heydenreich, F.M., Smit, M.J., et al. (2022). Computationally designed GPCR quaternary structures bias signaling pathway activation. *Nat. Commun.* 13, 6826. <https://doi.org/10.1038/s41467-022-34382-7>.
 29. Stephens, B., and Handel, T.M. (2013). Chemokine receptor oligomerization and allostericity. *Prog. Mol. Biol. Transl. Sci.* 115, 375–420. <https://doi.org/10.1016/B978-0-12-394587-7.00009-9>.
 30. Thelen, M., Muñoz, L.M., Rodríguez-Frade, J.M., and Mellado, M. (2010). Chemokine receptor oligomerization: functional considerations. *Curr. Opin. Pharmacol.* 10, 38–43. <https://doi.org/10.1016/j.coph.2009.09.004>.
 31. Martinez-Munoz, L., Rodriguez-Frade, J.M., Barroso, R., Sorzano, C.O.S., Torreno-Pina, J.A., Santiago, C.A., Manzo, C., Lucas, P., Garcia-Cuesta, E.M., Gutierrez, E., et al. (2018). Separating Actin-Dependent Chemokine Receptor Nanoclustering from Dimerization Indicates a Role for Clustering in CXCR4 Signaling and Function. *Mol. Cell* 70, 106–119. <https://doi.org/10.1016/j.molcel.2018.02.034>.
 32. Lao, J., He, H., Wang, X., Wang, Z., Song, Y., Yang, B., Ullahkhan, N., Ge, B., and Huang, F. (2017). Single-Molecule Imaging Demonstrates Ligand Regulation of the Oligomeric Status of CXCR4 in Living Cells. *J. Phys. Chem. B* 121, 1466–1474. <https://doi.org/10.1021/acs.jpcb.6b10969>.
 33. Mosi, R.M., Anastassova, V., Cox, J., Darkes, M.C., Idzan, S.R., Labrecque, J., Lau, G., Nelson, K.L., Patel, K., Santucci, Z., et al. (2012). The molecular pharmacology of AMD11070: an orally bioavailable CXCR4 HIV entry inhibitor. *Biochem. Pharmacol.* 83, 472–479. <https://doi.org/10.1016/j.bcp.2011.11.020>.
 34. García-Cuesta, E.M., Martínez, P., Selvaraju, K., Gómez Pozo, A.M., D'Agostino, G., Gardeta, S., Quijada-Freire, A., Blanco Gabella, P., Roca, C., Jiménez-Saiz, R., et al. (2024). Allosteric modulation of the CXCR4:CXCL12 axis by targeting receptor nanoclustering via the TMV-TMVI domain. *Elife* 13, RP93968. <https://doi.org/10.7554/elife.93968.1>.
 35. Janz, J.M., Ren, Y., Looby, R., Kazmi, M.A., Sachdev, P., Grunbeck, A., Haggis, L., Chinnapen, D., Lin, A.Y., Seibert, C., et al. (2011). Direct interaction between an allosteric agonist pepducin and the chemokine receptor CXCR4. *J. Am. Chem. Soc.* 133, 15878–15881. <https://doi.org/10.1021/ja206661w>.
 36. Lazim, R., Suh, D., Lee, J.W., Vu, T.N.L., Yoon, S., and Choi, S. (2021). Structural Characterization of Receptor-Receptor Interactions in the Allosteric Modulation of G Protein-Coupled Receptor (GPCR) Dimers. *Int. J. Mol. Sci.* 22, 3241. <https://doi.org/10.3390/ijms22063241>.
 37. Shen, S., Zhao, C., Wu, C., Sun, S., Li, Z., Yan, W., and Shao, Z. (2023). Allosteric modulation of G protein-coupled receptor signaling. *Front. Endocrinol.* 14, 1137604. <https://doi.org/10.3389/fendo.2023.1137604>.
 38. Lopez-Balastegui, M., Stepniewski, T.M., Kogut-Gunthel, M.M., Di Pizio, A., Rosenkilde, M.M., Mao, J., and Selent, J. (2024). Relevance of G protein-coupled receptor (GPCR) dynamics for receptor activation, signalling bias and allosteric modulation. *Br. J. Pharmacol.* <https://doi.org/10.1111/bph.16495>.
 39. Armando, S., Quoyer, J., Lukashova, V., Maiga, A., Percherancier, Y., Heveker, N., Pin, J.P., Prézeau, L., and Bouvier, M. (2014). The chemokine CXCR4 and CC2 receptors form homo- and heterooligomers that can engage their signaling G-protein effectors and betaarrestin. *Faseb. J.* 28, 4509–4523. <https://doi.org/10.1096/fj.13-242446>.
 40. Wouters, E., Vasudevan, L., Crans, R.A.J., Saini, D.K., and Stove, C.P. (2019). Luminescence- and Fluorescence-Based Complementation Assays to Screen for GPCR Oligomerization: Current State of the Art. *Int. J. Mol. Sci.* 20, 2958. <https://doi.org/10.3390/ijms20122958>.

41. Wang, J., He, L., Combs, C.A., Roderiquez, G., and Norcross, M.A. (2006). Dimerization of CXCR4 in living malignant cells: control of cell migration by a synthetic peptide that reduces homologous CXCR4 interactions. *Mol. Cancer Therapeut.* 5, 2474–2483. <https://doi.org/10.1158/1535-7163.MCT-05-0261>.
42. Hernanz-Falcon, P., Rodriguez-Frade, J.M., Serrano, A., Juan, D., del Sol, A., Soriano, S.F., Roncal, F., Gomez, L., Valencia, A., Martinez, A.C., and Mellado, M. (2004). Identification of amino acid residues crucial for chemokine receptor dimerization. *Nat. Immunol.* 5, 216–223. <https://doi.org/10.1038/ni1027>.
43. Percherancier, Y., Berchiche, Y.A., Slight, I., Volkmer-Engert, R., Tamamura, H., Fujii, N., Bouvier, M., and Heveker, N. (2005). Bioluminescence resonance energy transfer reveals ligand-induced conformational changes in CXCR4 homo- and heterodimers. *J. Biol. Chem.* 280, 9895–9903. <https://doi.org/10.1074/jbc.M411151200>.
44. Hamatake, M., Aoki, T., Futahashi, Y., Urano, E., Yamamoto, N., and Komano, J. (2009). Ligand-independent higher-order multimerization of CXCR4, a G-protein-coupled chemokine receptor involved in targeted metastasis. *Cancer Sci.* 100, 95–102. <https://doi.org/10.1111/j.1349-7006.2008.00997.x>.
45. Ge, B., Lao, J., Li, J., Chen, Y., Song, Y., and Huang, F. (2017). Single-molecule imaging reveals dimerization/oligomerization of CXCR4 on plasma membrane closely related to its function. *Sci. Rep.* 7, 16873. <https://doi.org/10.1038/s41598-017-16802-7>.
46. Liu, J., Tang, H., Xu, C., Zhou, S., Zhu, X., Li, Y., Prézeau, L., Xu, T., Pin, J.P., Rondard, P., et al. (2022). Biased signaling due to oligomerization of the G protein-coupled platelet-activating factor receptor. *Nat. Commun.* 13, 6365. <https://doi.org/10.1038/s41467-022-34056-4>.
47. Enten, G.A., Gao, X., McGee, M.Y., Weche, M., and Majetschak, M. (2024). Chemokine receptor hetero-oligomers regulate monocyte chemotaxis. *Life Sci. Alliance* 7, e202402657. <https://doi.org/10.26508/lsa.202402657>.
48. Babcock, G.J., Farzan, M., and Sodroski, J. (2003). Ligand-independent dimerization of CXCR4, a principal HIV-1 coreceptor. *J. Biol. Chem.* 278, 3378–3385. <https://doi.org/10.1074/jbc.M210140200>.
49. Weis, W.I., and Kobilka, B.K. (2018). The Molecular Basis of G Protein-Coupled Receptor Activation. *Annu. Rev. Biochem.* 87, 897–919. <https://doi.org/10.1146/annurev-biochem-060614-033910>.
50. Munoz, L.M., Holgado, B.L., Martinez, A.C., Rodriguez-Frade, J.M., and Mellado, M. (2012). Chemokine receptor oligomerization: a further step toward chemokine function. *Immunol. Lett.* 145, 23–29. <https://doi.org/10.1016/j.imlet.2012.04.012>.
51. Chen, Y., Li, Y., Zhou, Q., Cong, Z., Lin, S., Yan, J., Chen, X., Yang, D., Ying, T., and Wang, M.W. (2024). A homotrimeric GPCR architecture of the human cytomegalovirus revealed by cryo-EM. *Cell Discov.* 10, 52. <https://doi.org/10.1038/s41421-024-00684-x>.
52. Emsley, P., Lohkamp, B., Scott, W.G., and Cowtan, K. (2010). Features and development of Coot. *Acta Crystallogr. D Biol. Crystallogr.* 66, 486–501. <https://doi.org/10.1107/S0907444910007493>.
53. Liebschner, D., Afonine, P.V., Baker, M.L., Bunkóczki, G., Chen, V.B., Croll, T.I., Hintze, B., Hung, L.W., Jain, S., McCoy, A.J., et al. (2019). Macromolecular structure determination using X-rays, neutrons and electrons: recent developments in Phenix. *Acta Crystallogr. D Struct. Biol.* 75, 861–877. <https://doi.org/10.1107/S2059798319011471>.
54. Abraham, M.J., Murtola, T., Schulz, R., Páll, S., Smith, J.C., Hess, B., and Lindahl, E. (2015). GROMACS: High performance molecular simulations through multi-level parallelism from laptops to supercomputers. *SoftwareX* 1–2, 19–25. <https://doi.org/10.1016/j.softx.2015.06.001>.
55. Chun, E., Thompson, A.A., Liu, W., Roth, C.B., Griffith, M.T., Katritch, V., Kunken, J., Xu, F., Cherezov, V., Hanson, M.A., and Stevens, R.C. (2012). Fusion partner toolchest for the stabilization and crystallization of G protein-coupled receptors. *Structure* 20, 967–976. <https://doi.org/10.1016/j.str.2012.04.010>.
56. Duan, J., Shen, D.D., Zhou, X.E., Bi, P., Liu, Q.F., Tan, Y.X., Zhuang, Y.W., Zhang, H.B., Xu, P.Y., Huang, S.J., et al. (2020). Cryo-EM structure of an activated VIP1 receptor-G protein complex revealed by a NanoBIT tethering strategy. *Nat. Commun.* 11, 4121. <https://doi.org/10.1038/s41467-020-17933-8>.
57. Liu, A., Liu, Y., Llinàs Del Torrent Masachs, C., Zhang, W., Pardo, L., and Ye, R.D. (2024). Structural insights into KSHV-GPCR constitutive activation and CXCL1 chemokine recognition. *Proc. Natl. Acad. Sci. USA* 121, e2403217121. <https://doi.org/10.1073/pnas.2403217121>.
58. Liu, Y., Liu, A., Li, X., Liao, Q., Zhang, W., Zhu, L., and Ye, R.D. (2024). Cryo-EM structure of monomeric CXCL12-bound CXCR4 in the active state. *Cell Rep.* 43, 114578. <https://doi.org/10.1016/j.celrep.2024.114578>.

STAR★METHODS

KEY RESOURCES TABLE

REAGENT or RESOURCE	SOURCE	IDENTIFIER
Antibodies		
APC-labeled anti-CXCR4 antibody	Thermo Fisher Scientific	Cat# 17-9999-42 RRID:AB_1724113
Bacterial and virus strains		
<i>E. coli</i> DH5 α	NEB	Cat# C2988
Chemicals, peptides, and recombinant proteins		
Apyrase	Sigma	Cat# A6535
Protease Inhibitor Cocktail, EDTA-free	TargetMol	Cat# C0001
n-dodecyl- β -D-maltoside (DDM)	Anatrace	Cat# D310
Cholesteryl hemisuccinate (CHS)	Anatrace	Cat# CH210
Anti-DYKDDDK G1 Affinity Resin	GenScript Biotech	Cat# L00432
Lauryl maltose neopentylglycol (LMNG)	Anatrace	Cat# NG310
High Affinity Ni-Charged Resin FF	GenScript Biotech	Cat# L00666
SIM SF Expression Medium	SinoBiological	Cat# MSF1
DMEM	Gibco	Cat# 11965092
Characterized Fetal Bovine Serum (FBS), New Zealand Origin	HyClone	Cat# SH30406.05
HBSS, Calcium, magnesium	Gibco	Cat# 14025-092
Human CXCL12	PeproTech	Cat# 30028A
FLAG peptide	GenScript	Custom Synthesis
Lipofectamine 3000	Invitrogen	Cat# L3000001
Forskolin	MCE	Cat# HY-15371
Coelenterazine H	Yeasen Biotech	Cat# 40906ES
Critical commercial assays		
ClonExpress Ultra One Step Cloning Kit	Vazyme Biotech	Cat# C115
Bac-to-Bac Expression System	Invitrogen	Cat# A11098
LANCE Ultra cAMP kit	PerkinElmer Life Sciences	Cat# TRF0263
Deposited data		
CXCR4 tetrameric complex EM map	This work	EMDB: EMD-39573
CXCR4 tetrameric complex coordinates	This work	PDB: 8YU7
Experimental models: Cell lines		
<i>Spodoptera frugiperda</i> Sf9 insect cell line	Invitrogen	Cat# 11496015
HeLa cell line	ATCC	Cat# CCL2
HEK293T cell line	ATCC	Cat# CRL-3216
Recombinant DNA		
pFastBac-FLAG-CXCR4	This work	N/A
pFastBac-CXCL12	This work	N/A
pFastBac-beta-arrestin1	This work	N/A
pcDNA3.1-CXCR4-WT	This work	N/A
pcDNA3.1-CXCR4-V1	This work	N/A
pcDNA3.1-CXCR4-V2	This work	N/A
pcDNA3.1-CXCR4-RLN	This work	N/A
pcDNA3.1-CXCR4-RLC	This work	N/A
pcDNA3.1-CXCR4-K38A	This work	N/A
pcDNA3.1-CXCR4-V1-K38A	This work	N/A

(Continued on next page)

Continued

REAGENT or RESOURCE	SOURCE	IDENTIFIER
pcDNA3.1-CXCR4-V2-K38A	This work	N/A
pcDNA3.1-CXCR4-RLN-K38A	This work	N/A
pcDNA3.1-CXCR4-RLC-K38A	This work	N/A
pcDNA3.1-CXCR4-V99A	This work	N/A
pcDNA3.1-CXCR4-V1-V99A	This work	N/A
pcDNA3.1-CXCR4-V2-V99A	This work	N/A
pcDNA3.1-CXCR4-RLN-V99A	This work	N/A
pcDNA3.1-CXCR4-RLC-V99A	This work	N/A
pcDNA3.1-CXCR4-Q272A	This work	N/A
pcDNA3.1-CXCR4-V1-Q272A	This work	N/A
pcDNA3.1-CXCR4-V2-Q272A	This work	N/A
pcDNA3.1-CXCR4-RLN-Q272A	This work	N/A
pcDNA3.1-CXCR4-RLC-Q272A	This work	N/A
Software and algorithms		
cryoSPARC v3.3.1	Structura Biotechnology	https://cryosparc.com/
Chimera	UCSF	https://www.cgl.ucsf.edu/chimera/
ChimeraX	UCSF	https://www.cgl.ucsf.edu/chimerax/
COOT	Emsley et al. ⁵²	https://www2.mrc-lmb.cam.ac.uk/personal/pemsley/coot/
Phenix	Liebschner et al. ⁵³	https://phenix-online.org/
CHARMM-GUI	Lehigh University	https://www.charmm-gui.org/
GROMACS	Abraham et al. ⁵⁴	https://www.gromacs.org/
PyMOL	Schrödinger	https://pymol.org/2/
GraphPad Prism	GraphPad	https://www.graphpad.com/
Other		
Amicon Ultra Centrifugal Filters-100k	Millipore	Cat# UFC9100
Superose 6 Increase 10/300GL column	GE Healthcare	Cat# 29091596
Superdex 200 Increase 10/300 column	GE Healthcare	Cat# 28990944
Quantifoil Au 300 mesh R1.2/1.3 grids	Sigma	Cat# TEM-Q350AR1.3

EXPERIMENTAL MODEL AND STUDY PARTICIPANT DETAILS

Spodoptera frugiperda (Sf9) cells (ATCC CRL-1711) tested negative for mycoplasma were used for virus production. The cells were cultured in SIM SF Expression Medium (SinoBiological, Beijing, China) at 27°C with agitation at 120 rpm. For functional assays, HeLa cells (ATCC CCL-2) and HEK293T cells (ATCC CRL-3216), both tested negative for mycoplasma, were cultured in a humidified incubator at 37°C with 5% CO₂, using DMEM medium (Gibco) supplemented with 10% fetal bovine serum (HyClone).

METHOD DETAILS

Constructs

The coding sequence of wild-type human CXCR4 was synthesized by General Biol (Chuzhou, China) and was cloned into the pFast-Bac plasmid (Invitrogen, Carlsbad, CA). A hemagglutinin (HA) signal peptide followed by an FLAG tag was fused at the N terminus to facilitate protein expression and purification.^{55,56} For plasmid constructs of the complementary BRET assay,⁴⁰ the coding sequences of CXCR4, V1 (1–210 of mVenus), V2 (211–238 of mVenus), RLN (1–228 of Renilla luciferase) and RLC (229–311 of Renilla luciferase) were PCR amplified (2 × Phanta Max Master Mix, Vazyme Biotech, Shanghai, China; Cat# P515) and assembled into pcDNA3.1(+) plasmids. All plasmid constructs were verified for accuracy by DNA sequencing (Genewiz, Suzhou, China).

Protein expression

For structural determination, we use the insect Sf9 cell (*Spodoptera frugiperda*) and baculovirus expression system (Invitrogen) for protein expression as we reported before.^{57,58} The baculovirus vectors containing CXCR4, CXCL12 and β-arrestin1 were prepared according to instructions of the bac-to-bac expression system (Invitrogen). Sf9 insect cells were grown in suspension at 27°C. When

density reached 2×10^6 cells per mL, the cells were infected by the prepared baculoviruses of CXCR4, CXCL12 and beta-arrestin1 with MOI (multiplicity of infection) at 2, 0.5 and 1 respectively. After infection, the cells were allowed to grow for 48 h. Then, the cells were collected by centrifugation and stored at -80°C until use.

Complex purification

Frozen cell pellets from 4 L of culture were thawed and resuspended in the buffer containing 20 mM HEPES pH 7.4, 50 mM NaCl, 5 mM KCl, 5 mM MgCl₂, 5 mM CaCl₂, with 100 × concentrated EDTA-free protease inhibitor cocktail (TargetMol). Subsequently, 0.8% (w/v) Lauryl Maltose Neopentyl Glycol (LMNG, Anatrace) and 0.2% (w/v) cholesteryl hemisuccinate (CHS, Anatrace) were added to solubilize complexes for 2 h at 4°C . Insoluble material was removed by centrifugation at 30,000 × g for 40 min. The supernatant was collected and incubated with anti-FLAG affinity resin (GenScript Biotech, Piscataway, NJ). Then, the resin was loaded onto a gravity-flow column. After that, the resin in the gravity-flow column was washed with 20 column volumes of buffer containing 100 mM NaCl, 2 mM CaCl₂, 2 mM MgCl₂, 0.05% (w/v) LMNG, 0.003% (w/v) CHS. The protein complex was eluted with buffer containing 20 mM HEPES pH 7.4, 100 mM NaCl, 2 mM CaCl₂, 2 mM MgCl₂, 0.01% (w/v) LMNG, 0.001% (w/v) CHS, 0.2 mg/mL FLAG peptide (Sigma-Aldrich). The elution was concentrated to 500 μL in an Amicon Ultra-15 Centrifugal Filter Unit (Millipore, Burlington, MA), and then loaded onto a Superose 6 Increase 10/300GL column (GE Healthcare) with running buffer containing 20 mM HEPES pH 7.4, 100 mM NaCl, 0.00075% (w/v) LMNG, 0.0002% (w/v) CHS. The peak fraction of the complex was pooled and concentrated to approximately 10 mg/mL, and then flash-frozen in liquid nitrogen. The purified protein complex was stored at -80°C until further use.

Cryo-EM grid preparation

The Ultrafoil 300 mesh R1.2/1.3 holy Au grids were used for preparation of cryo-EM grids. The grids were glow-discharged by Tergeo-EM plasma cleaner. Afterward, aliquots of 3 μL purified complex were loaded at 4°C in 100% humidity. Then, the grids were blotted by the filter papers for 3.5 s with a blot force of 1 and plunge-frozen in liquid ethane immediately. The Cryo-EM grid preparation was operated using Vitrobot Mark IV (Thermo Fisher Scientific, Waltham, MA). The prepared grids were stored in liquid nitrogen until further use.

Cryo-EM data collection

Cryo-EM imaging was taken by a Titan Krios electron microscope operated at 300 kV using a Gatan K3 Summit detector. The Cryo-EM grids were screened for data collection. The data was acquired at a nominal magnification of 105,000 and the pixel size of the image is 0.85 Å. Inelastically scattered electrons were excluded by a GIF Quantum energy filter (Gatan, USA) using a slit width of 20 eV. Data collection was performed by the semi-automatic data acquisition software SerialEM (Mastronarde, 2005) and the defocus range was set from -1.2 to -2.5 μm . The dataset was collected in electron counting mode and 7,613 image stacks were obtained in 72 h. The total exposure time of each stack is 2.5 s, which is fractionated to 50 frames at a dose rate of 20.1 e/pixel/s.

Cryo-EM image processing and 3D reconstruction

The Cryo-EM image processing and 3D reconstruction were performed mainly using the software cryoSPARC v3.3.1 (Structura Biotechnology Inc., Toronto, Canada). The image stacks were first subjected to patch motion correction with electron dose-weighting. Then, patch CTF estimation was used to estimate CTF parameters. The resulting micrographs were manually inspected, and those with clear defects, such as ice contamination or deviation from the sample hole, were discarded. A small dataset of 2,338 particles was manually picked and used to generate auto-picking templates through 2D classification. Subsequently, a total of 1,626,680 particles were auto-picked. Multiple rounds of 2D classification were then performed to screen particles. Particles within 2D classes exhibiting well-defined features were selected, resulting in a dataset of 415,809 particles after five rounds of 2D classification. *Ab initio* reconstruction was then applied to generate an initial 3D model, followed by 3D classification to select homogeneous particles, resulting in a final particle dataset containing 80,835 particles.

The final dataset was used for homogeneous refinement, particle polish, non-uniform refinement, and local refinement, yielding a map with a global resolution of 3.21 Å, which was estimated at a Fourier shell correlation of 0.143. The map revealed a potential C4 symmetry. To improve map quality, C4 symmetry was applied, upgrading the final resolution to 3.01 Å. The overall geometry remained unchanged when compared to the C1 map (Figure S3B).

Model building and refinement

The predicted model of the CXCR4 receptor from the AlphaFold Protein Structure Database at code AF-Q96P68-F1, was used as a starting template for model building. UCSF Chimera-1.1470 was used to dock the model into the electron microscopy density map. The model was then manually rebuilt and adjusted against the electron microscopy density map in COOT-0.9.8, as well as iterative refinement by Phenix-1.2073 programs. The models were further validated by Molprobity, and the statistics were provided in Table S1. The structural figures were generated using UCSF Chimera-1.14, ChimeraX-1.274 and PyMOL-2.0.

Complementary BRET assay

A complementary BRET assay was developed by using RLuc as the BRET donor which was separated into an N-terminal fragment (RLN) and a C-terminal fragment (RLC), both fused to the C terminus of CXCR4. The fluorescent protein mVenus was used as the

BRET acceptor, which was separated into V1 and V2 fragments and connected to the C terminus of CXCR4.^{39,40} HeLa cells were transfected with plasmids encoding WT/mutant CXCR4-V1, WT/mutant CXCR4-V2, WT/mutant CXCR4-RLN, and WT/mutant CXCR4-RLC together. After 24 h of incubation, the cells were collected for complementary BRET assay. BRET signals were recorded using an EnVision 2105 multimode plate reader (PerkinElmer Waltham, MA) 30 min after the addition of the luciferase substrate coelenterazine H (Yeasen Biotech, Shanghai, China) to a final concentration of 5 µM. BRET signals were derived from the emission at 525 nm divided by the emission at 460 nm. Baseline BRET signals were collected for 2 min. After the addition of CXCL12 at different concentrations, BRET signals were collected for another 10 min. The difference in BRET ratio was calculated as $\Delta\text{BRET} = (\text{average BRET}_{\text{after stimulation}}) - (\text{average BRET}_{\text{before stimulation}})$.

Surface expression analysis

HEK293T cells were transfected with wild-type or mutant CXCR4 expression vectors for 24 h. Cells were then harvested and washed in HBSS, then incubated with an APC labeled anti-CXCR4 mAb (12G5; Thermo Fisher Scientific, Cat #17-9999-42; 1:50 dilution in HBSS buffer) for 30 min on ice. Fluorescence signals indicating the cell surface expression of CXCR4 were quantified by flow cytometry (CytoFLEX, Beckman Coulter, Brea, CA).

cAMP inhibition assay

For the cAMP inhibition assay, wild-type CXCR4 and its mutants (K38A, V99A, and Q272A) were transiently expressed in HeLa cells 24 h before the experiment. The cells were resuspended in HBSS stimulation buffer containing 5 mM HEPES, 0.1% BSA (w/v), and 0.5 mM 3-isobutyl-1-methylxanthine (IBMX). Various concentrations of CXCL12 (Cat# 30028A; Peprotech, Rocky Hill, NJ) were prepared in the same stimulation buffer. Cells were then treated with 2.5 µM forskolin and CXCL12 at different concentrations for 30 min in an incubator. Intracellular cAMP levels were measured using the LANCE Ultra cAMP kit (Cat# TRF0263; PerkinElmer Life Sciences, Waltham, MA), according to the manufacturer's protocol. Time-resolved fluorescence resonance energy transfer (TR-FRET) signals were detected using an EnVision 2105 multimode plate reader (PerkinElmer). Intracellular cAMP concentrations were calculated as per the manufacturer's instructions.

QUANTIFICATION AND STATISTICAL ANALYSIS

Statistical analyses were conducted using Prism 9.5.0 (GraphPad, San Diego, CA). Dose-response curves were generated using the log[agonist] vs. response equation (three parameters) within the software. Results are expressed as mean ± SEM, derived from at least three independent experiments.